INVENTORY OF SUPPLEMENTAL INFORMATION

We provide 4 supplemental figures to our manuscript. The relationship of these figures to those that appear in the body of the manuscript is outlined below:

Figure S1 provides validation of the parabiosis model as well as an indication of the blood-spinal cord barrier disruption and astrocyte response that accompanies it. Figure S1 is thus an accompaniment to Figure 1, which provides an overview of the precursor cell and angiogenic responses to parabiosis.

Figure S2 is directly linked to Figure 2. Fig.S2A corroborates the findings of Fig.2A using transferrin as an independent oligodendrocyte marker. Fig.S2B demonstrates that the differences identified in remyelination between isochronic-old and heterochronic-old lesions, as delineated in Fig.2, were not attributed to differences in lesion volume.

Figures S3 and **S4** provide supplemental information to Figure 4. Fig.4 presents evidence for the importance of MCP-1/CCR2 axis and young-partner derived monocytes/macrophages in the rejuvenation of remyelination observed in parabiosis. Fig.S3A demonstrates that oligodendrocyte densities are lower in the remyelinating lesions of single CCR2 deficient mice, confirming the importance of CCR2-dependent processes in remyelination. Fig.S3B demonstrates that cross-circulation is not impaired in parabiosis in the setting of CCR2 deficiency. As is demonstrated in Fig.4, not all of the rejuvenating effects of heterochronic parabiosis on remyelination can be attributed to CCR2-dependent mechanisms, implicating non-cell mediated factors. As is seen in Fig.S4 we were not able to detect differences in monocyte growth factor expression, nor in systemic cytokine profiles, to account for this effect.

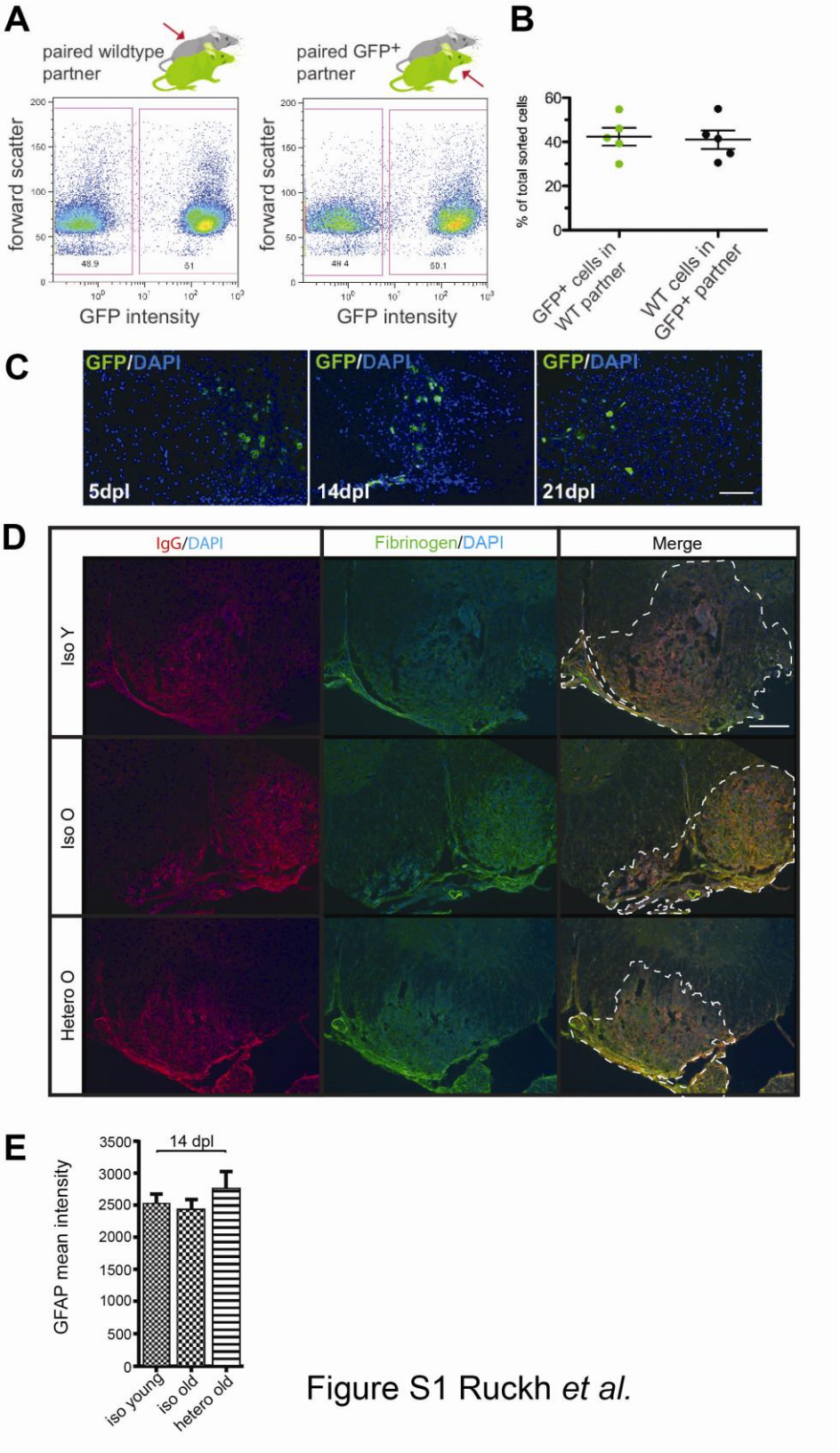

Figure S1 Ruckh *et al.*

Figure S1: Lesions in old mice are exposed to young systemic environment. Related to Figure 1. **(A)** Flow cytometry analysis of splenocytes from parabiotic pairs indicating chimerism of GFP-labeled populations. Percentages of each population are indicated in respective gates. **(B)** Quantification of cross-circulation. Data are presented as mean ± SEM for each group (n=5). **(C)** Young donor-derived cells infiltrate lesions in old partners. 3 heterochronic GFP+/WT pairs were analyzed for each timepoint, and representative fields are shown for lesions at 5, 14 and 21dpl. The hypercellular area indicates the lesion. GFP^+ cells were detected in old parabiotic partner lesions at each survival time, confirming perfusion by young blood. **(D)** immunohistochemcial detection of IgG and Fibrinogen within lesion spinal cord in isochronic young (Iso Y), isochronic old (Iso O) and heterochronic (Hetero O) pairings reveals disruption of the blood-spinal cord barrier. Dashed line indicates lesion boundary. Note the absence of IgG or Fibrinogen staining outside the lesion where the blood-spinal cord barrier remains intact. Representative images. **(E)** Quantification of GFAP staining in the lesions of isochronic-young, isochronic-old and heterochronic-old animals at 14dpl to assess astrocytosis after experimentally induced demyelination. No significant difference between the groups was detectable. Data are displayed as mean ± SEM. Scale bars: C 100µm, D 200µm.

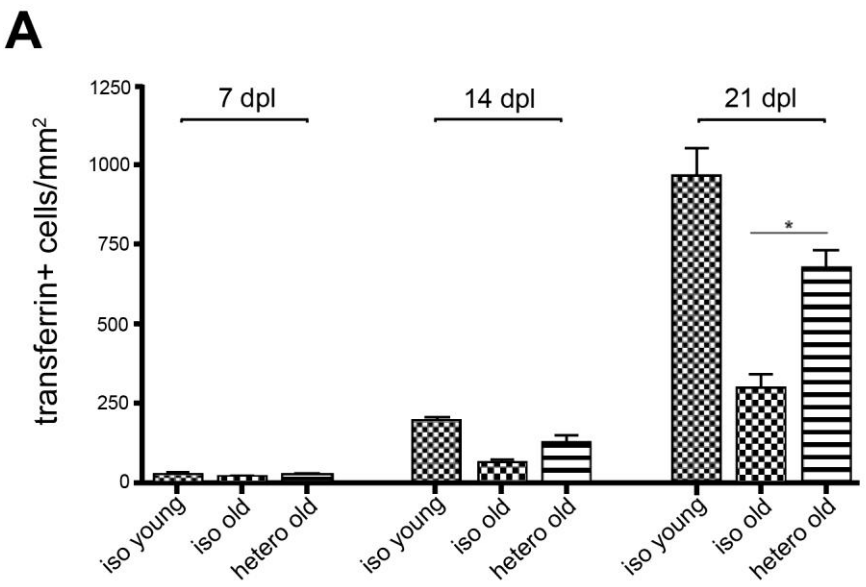

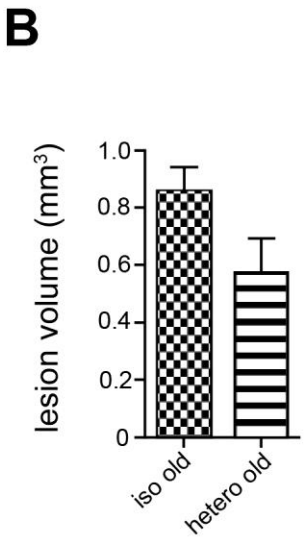

Figure S2 Ruckh *et al.*

Figure S2: Heterochronic parabiosis stimulates OPC differentiation and remyelination. Related to Figure 2. **(A)** Quantification of mature oligodendrocytes using an independent marker, transferrin, to confirm loss of oligodendrocytes in the lesion at 7dpl and their subsequent new generation (n≥4). Use of this marker also confirms the significant increase in differentiated oligodendrocytes in heterochronic-old animals at 21dpl. **(B)** Lesion size does not differ between old animals in isochronic and heterochronic parabiotic pairings. Lesion volume was quantified in isochronic-old (n=3) and heterochronic-old animals (n=4) by analyzing serial sections spanning the entire lesion in equidistant spacing, and doing a volumetric reconstruction of the lesion. Lesion size was not detectably different between these two groups. Data for (A) and (B) are presented as mean ± SEM.

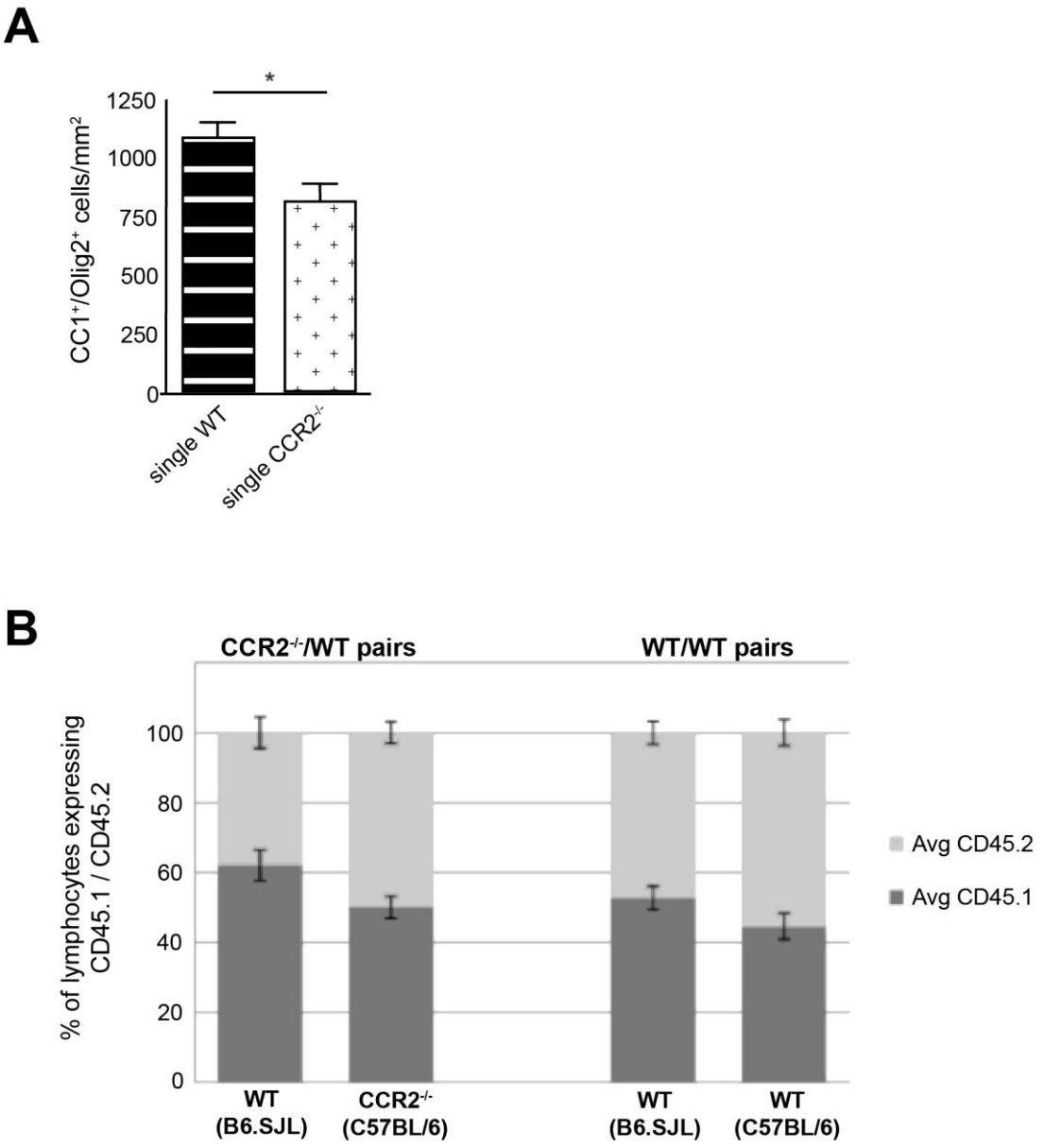

Figure S3 Ruckh *et al.*

Figure S3: Engrafted cells in the spinal cord lesions of parabionts are chiefly young-partner derived macrophages. Related to Figure 4. **(A)** At 21 dpl the density of $CC1^{+}/Olig2^{+}$ cells (mature oligodendrocytes within areas of lysolecithin-induced demyelination is significantly reduced in young adult $CCR2^{-/-}$ mice compared to wild type mice of similar background (n=4 per group). Data are presented as mean ± SEM. **(B)** CCR2-deficiency of one partner does not affect cross-circulation during parabiosis. Blood samples were collected from each partner of heterochronic WT^{young}/WT^{old} pairs (n=4) and CCR2-KO^{young}/WT^{old} pairs (n=4) 7 days after joining and analysed for the expression of CD45.1 and CD45.2 on lymphocytes by FACS. Data are displayed as mean percentage ± SD of leukocytes that are positive for CD45.1 and CD45.2, respectively, in each partner. Levels of blood chimerism in CCR2-KO^{young}/WT^{old} pairs were found to be comparable to WT^{young}/WT^{old} control pairs, indicating that cross-circulation is established to full extent without delay despite the CCR2-deficiency of one partner.

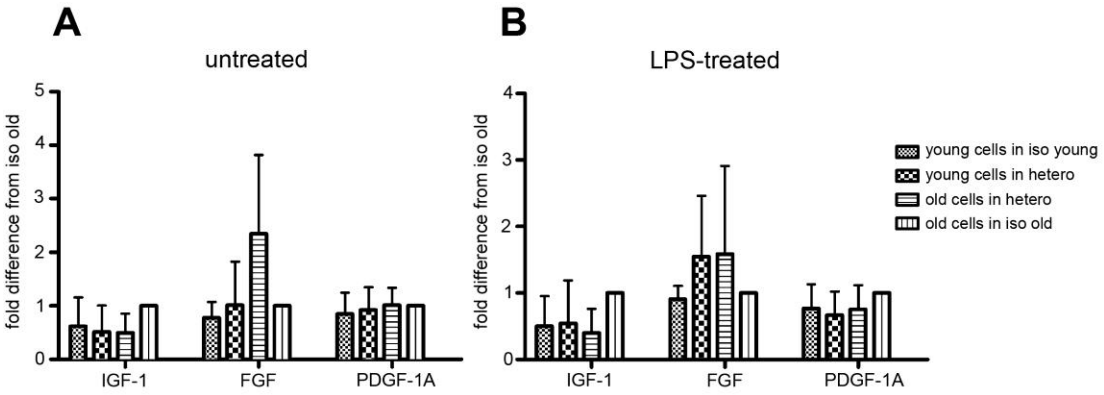

C

6Ckine	E-Selectin	IL-2	JAM-A	Pro-MMP-9
ALK-1	Fas Ligand	IL-2 R alpha	KC	RANTES
Amphiregulin	Fcg RIIB	IL-3	Leptin	SCF
Axl	Flt-3 Ligand	IL-4	Leptin R	sTNF RI
BLC	Fractalkine	IL-5	L-Selectin	sTNF RII
Cardiotrophin-1	Galectin-1	IL-6	Lungkine	TACI
CD27	Gas 6	IL-9	Mad CAM-1	TARC
CD27 L	GCSF	IL-10	MCP-1	TNF alpha
CD30	GITR	IL-11	MDC	TPO
CD30 L	GITR Ligand	IL-12 p40	MFG-E8	TRANCE
CD36/SR-B3	Granzyme B	IL-12 p70	MIG	TROY
CTLA-4	HAI-1	IL-13	MIP-1alpha	TWEAK R
CXCL16	HGF	IL-15	MIP-1gamma	VCAM-1
Decorin	IFN gamma	IL-17	MIP2	VEGF
Dkk-1	IGFBP-5	IL-17B R	MIP-3 alpha	VEGF R1
E-Cadherin	IGFBP-6	IL-17E	MIP-3 beta	VEGF R3
EGF	IGF-II	IL-17F	MMP-2	VEGF-D
Eotaxin	IL-1 alpha	IL-20	Osteopontin	
Eotaxin-2	IL-1 beta	IL-21	Osteoporotegerin	
Epigen	IL-1ra	I-TAC	Prolactin	

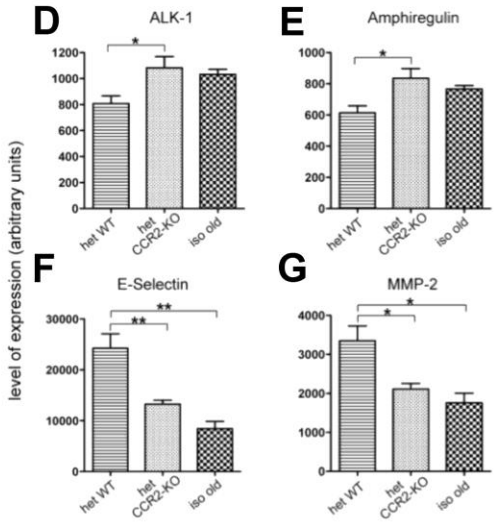

Figure S4 Ruckh *et al.*

Figure S4: Young macrophages play a central role in the rejuvenating effect of heterochronic parabiosis. Related to Figure 4. **(A-B)** Bone marrow derived macrophages cultured from isochronic or heterochronic parabionts produce equivalent amounts of IGF-1, FGF, and PDGF-1A. CD45+ bone marrow cells were sorted by FACS from both young partners of isochronic-young pairs (young cells in iso young), from the young or old partner of heterochronic pairs (young cells in hetero and old cells in hetero, respectively), or from both partners of isochronic-old pairs (old cells in iso old). Cells were cultured *in vitro* for 7 days (see Supplemental Methods for details), under conditions that stimulate macrophage differentiation. Macrophage differentiation was confirmed by flow cytometric staining, which indicated that cultures contained an average of 81 ± 11.6% (mean ± SD) $CD11b^{+}F4/80^{+}$ macrophages. Conditioned supernatant from these culture-derived macrophages was harvested directly (A) or following stimulation of macrophages for 6 hours with lipopolysaccharaide (LPS) (B). Supernatants were analyzed by ELISA for the presence of IGF-1, PDGF-1A or FGF. Data pooled from two independent experiments are plotted as the fold difference, compared to growth factor levels in macrophages from isochronic-old mice. Differences were not statistically significant, as determined by one-way ANOVA (Kruskal-Wallis with Dunn's multiple comparison post-test). **(C-G)** Cytokine array analysis of serum collected from parabiotic mice. Relative levels in serum of each of the indicated cytokines were determined by quantitative dot blot analysis. Samples were collected from isochronic-old pairs (iso-old, n=2 pairs), or from heterochronic pairs in which the young partner was wildtype (het WT, n=4 pairs) or deficient in CCR2 (het CCR2-KO, n=3 pairs). **(C)** Summary of data indicating the 4 cytokines (highlighted in grey) that showed a statistically significant difference ($p<0.05$ by one-way ANOVA) in the circulation of heterochronic WT vs. CCR2-KO containing pairs. Levels of all other cytokines were indistinguishable between these two groups ($p>0.05$). **(D-G)** Of the 4 cytokines – ALK-1 (D), Amphiregulin (E), E-Selectin (F), and MMP-2 (G) that showed significant differences in heterochronic pairs containing a CCR2-KO young partner, only E-selectin (F) and MMP-2 (G), were significantly different between WT heterochronic pairs and isochronic-old pairs. Data represent volumetric measurements (in arbitrary units) for the indicated cytokines and are presented as mean ± SEM. *$p<0.05$, **$p<0.01$ by one-way ANOVA.

SUPPLEMENTAL EXPERIMENTAL PROCEDURES

Animals. C57BL/6 ('wildtype', WT) mice, C57BL/6-UBC-GFP transgenic mice as well as the $CCR2^{-/-}$ mouse strain (Boring et al., 1997) on the C57BL/6 background were obtained from Jackson Laboratories (US). Parabiotic pairs with a GFP^{+} partner were generated with either C57BL/6-UBC-GFP transgenic mice or C57BL/6-β-actin-EGFP transgenic mice (Wright et al., 2001). $CCR2^{-/-}GFP^{+}$ mice were generated by crossing the $CCR2^{-/-}$ with ubc-GFP transgenic mice. For chimerism analysis, $CCR2^{-/-}$ mice were joined to B6.SJL mice (a congenic strain on the C57BL/6 background, carrying the CD45.1 allele), which also were obtained from Jackson Laboratories (US). For analysis of growth factor expression by bone marrow derived macrophages, C67BL/6 mice (from the National Institutes of Aging) were joined to each other or to B6.SJL mice (from Jackson Laboratories). Parabiosis and spinal cord injections on parabiosed mice were performed at the Joslin Diabetes Center animal facility, Boston, MA and at the BRI animal facility in the Department of Stem Cell and Regenerative Biology, Harvard University, Cambridge. All experiments were performed in compliance with the guidelines set by the Institutional Animal Care and Use Committee (IACUC) of Joslin Diabetes Center and Harvard University.

Parabiosis. Parabiotic pairs were joined as previously described (Wagers et al., 2002). All animals used for parabiotic pairings were female, from either isogenic or congenic strains to avoid immune rejection between the partners. Most parabiotic pairings included isochronic-young pairs (two young mice joined, each 5-7 weeks old), isochronic-old pairs (two old mice joined, each 10-12 months old) and heterochronic pairs (a young mouse joined to an old one, respective ages same as above). For analysis of growth factor expression by bone marrow derived macrophages, mice were joined at 2 months of age (young) and 22 months of age (old).

Induction of focal demyelination. Mice were anaesthetised by inhalation of isoflurane (for experiments on single mice) or by intraperitoneal injection of Avertin (tribromoethanol; for experiments on parabiotic mice). A focal demyelinating spinal cord lesion was induced as previously described (Woodruff et al., 2004). Briefly, the spinal

cord was exposed between two vertebrae of the thoracic column and 1μl of a 1% lysolecithin solution (L-α-lysophosphatidylcholine, Sigma) was injected into the ventral funiculus to create a reproducible ellipsoid-shaped demyelinating lesion. For lesions induced in parabiotic mice, lysolecithin was injected into one partner only at three weeks after parabiotic joining. Animals were maintained in the parabiotic state until sacrifice, at the post-lesion time points indicated.

Flow cytometry analysis of cross-circulation. Spleens were removed from both partners of GFP^+/WT parabiotic pairs at the point of sacrifice directly before perfusion. The tissue was homogenised, and red blood cells lysed by a 3min incubation with ACK buffer (0.15M Ammonium chloride, 0.01M Potassium bicarbonate) on ice. The cells were washed in staining medium (HBSS containing 2% FBS), and resuspended at a concentration of 10^8 cells/ml in staining medium. The suspension was then filtered through a 70μm cell strainer to remove aggregates. One aliquot of each splenocyte sample was mixed with 10μl of a 20μg/ml propidium iodide (PI) solution to label dead cells, which were excluded from analysis. Samples were analyzed by flow cytometry, using a Coulter EPICS XL-MCL (Beckman-Coulter), provided by the Joslin Diabetes Center Flow Cytometry Core. 10,000 events were acquired for each sample, and flow cytometry data was analyzed using FlowJo software (TreeStar, US).

Immunohistochemistry and quantification of immunolabelling. After perfusion-fixation via the left ventricle with 4% paraformaldhyde, spinal cords were dissected and cryosectioned. The lesion was identified as an area of hypercellularity in the normally hypocellular white matter. 12μm thick sections containing lesions of maximum diameter (representing the approximate centre of the lesion) were used for immunohistological analysis.

After blocking with donkey or goat serum and permeabilisation with 0.3% Triton-X 100 (Sigma), the sections were incubated overnight with the primary antibodies. Secondary antibodies were added for 1h at room temperature. For staining with the anti-Olig2, anti-Ki67 and anti-NKx2.2 antibodies, antigen retrieval was performed using Real Target Retrieval solution (Dako) prior to the protocol described above. For staining with the

mouse primary antibody anti-Nkx2.2, the Mouse-on-Mouse immunodetection kit (Vector laboratories, BMK-2202) was used according the manufacturers' instructions, and additional labelling with other antibodies or TUNEL was carried out subsequently.
For CD34 immunostaining, slides were pretreated with ice-cold methanol for 10min before blocking. Nuclei were counterstained with DAPI contained in the mounting medium (Vectashield, Vectorlabs). Immunostained sections were visualized on a Zeiss Observer.A1 Axio fluorescence microscope, and images acquired and analyzed using AxioVision software (Zeiss).

For quantification, cells of interest were counted in three different sections (each approximately 50μm apart) for each animal. To account for the varying size of the lesion in different sections, cell densities were calculated rather than using absolute cell numbers for the analysis.

Antibodies. The following primary antibodies were used: anti-Nkx2.2 (mouse, 1:100, Developmental Studies Hybridoma Bank), anti-Ki67 (rabbit, 1:400, Thermo Scientific, RM-9106), anti-CD34 (rat, 1:50, Abcam, ab8158), anti-GFAP (rabbit, 1:1000, DAKO, Z0334), anti-Olig2 (rabbit, 1:1000, Chemicon, AB9610), anti-CC1 (mouse, 1:300, Calbiochem, OP80), anti-transferrin (rabbit, 1:1000, Chemicon), anti-Mac1/CD11b (rat, 1:400, Serotec, MCA711), anti-CD4 (rat, 1:100, BioLegend, 100415), anti-CD8 (rat, 1:100, Santa Cruz Biotechnology, sc-18860), anti-CD94 (rat, 1:200, Serotec, MCA2288), biotinylated anti-B220 (rat, 1:100, BD Pharmingen, 553085), anti-neutrophil (NIMP-R14, rat, 1:100, Abcam, ab2557), anti-GFP Alexa Fluor 488-conjugated (rabbit, 1:800, Molecular Probes, A21311), anti-fibrinogen (sheep, AbD Serotec, 4440-8004), anti-degraded myelin basic protein antibody (rabbit, 1:500, Chemicon AB 5864) and anti-GFP (goat, 1:400; Abcam 5450). Additionally, the biotin-conjugated isolectin IB4 (1:100, Sigma-Aldrich, L-2140) was used. Anti-mouse IgG Alexa Fluor 594-conjugated antibody (donkey, 1:500, Molecular Probes, A-21203) was used for the analysis of extravasated IgG. The following secondary antibodies were used: donkey anti-rabbit AlexaFluor 488, donkey anti-goat AlexaFlour 488, donkey anti-mouse AlexaFluor 594, donkey anti-sheep Alexa Fluor 488, goat anti-mouse $IgG2_b$ AlexaFluor 594 (all from Molecular Probes), donkey anti-rabbit Cy3 and donkey anti-rat Cy3 (both from Jackson Immuno Research).

All secondary antibodies were used at a dilution of 1:500. For biotinylated primary antibodies or IB4, streptavidin 594 (Molecular Probes) was used at a dilution of 1:1000.

OPC apoptosis assay. To identify apoptotic OPCs, sections were sequentially labelled for Nkx2.2 and TUNEL. NKx2.2 immunostaining was performed as described above, followed by TUNEL assay using the In situ cell death detection kit (Roche, 11684795910) according to the manufacturer's protocol.

Oil Red-O staining. To detect lip-rich myelin debris, tissue sections were stained in prewarmed 0.5% Oil Red O (Sigma O-0625) dissolved in propylene glycol for 8 min at 60 degrees, and then differentiated in 85% propylene glycol for 3 minutes followed by a rinse in distilled water.

Ranking analysis of remyelination. In order to compare the extent of remyelination, a ranking analysis of the extent of remyelination was performed. Following perfusion-fixation via the left ventricle with 4% glutaraldehyde, the part of the spinal cord containing the lesion was dissected and embedded in TAAB resin. Semi-thin sections (1μm) were cut from the resin-embedded tissue using a microtome (Reichert-Jung) with glass knives. Sections were stained with toluidine Blue to achieve good contrast for histological analysis under a light microscope (Nikon Optiphot-2). Semi-thin resin sections that contained a lesion with maximum diameter (approximately representing the lesion centre) were selected for each animal and blindly ranked according to the extent of remyelination that was observed in the lesion using standard morphological criteria as previously described (Arnett et al., 2004). This method allowed the detection of statistically significant differences in the extent of remyelination between two groups, but did not indicate the overall extent of remyelination or the degree of the difference. More quantitative evidence of the extent of remyelination was provided by immunofluorescent staining for CC1 and transferrin, which correlate well with the extent of new myelin sheath formation at late stages of remyelination (21 dpl).

Lesion volume. Mice were perfused with 4% paraformaldehyde 5 days post lesion and their spinal cords were dissected. Serial 12μm thick transverse cryosections of the entire

lesion were cut and collected. Every tenth section was stained with DAPI to enable identification of the lesion as an area of hypercellularity in the hypocellular white matter. These stained sections were visualized on a Zeiss Observer.A1 Axio fluorescence microscope, and the lesion area was measured in each section using the AxioVision software (Zeiss). To reconstruct the total volume of the lesion, the quantified area was then averaged between adjacent sections, and the volume calculated using the known distance between them. These partial volumes were then added to calculate the total volume of the lesion.

Cytokine Arrays. Blood samples were collected from each partner of the parabiotic pair directly before perfusion. Samples were collected from 2 isochronic-old pairs (n=4 samples), 4 heterochronic pairs in which the young partner was wild-type (n=8 samples), and 3 heterochronic pairs in which the young partner was deficient in CCR2 (n=6 samples). After coagulation, samples were centrifuged for 15min at 8000rpm to isolate the serum. Per manufacturer guidelines, the RayBio Mouse Cytokine Antibody Array 6 (RayBiotech, Inc) was used to simultaneously detect the presence/absence of 97 cytokines in each of the serum samples. Detection was performed with a chemiluminescence imaging system (BioRad) and images were quantified using Quantity One (BioRad) Volume Analysis, followed by normalization using the RayBiotech Analysis Tool (RayBiotech, Inc.). As expected given their shared circulatory system, initial evaluation of the data revealed no differences in serum cytokine levels between the two partners of each parabiotic pair. Therefore, for all parabiotic groups, individual samples from each pair were considered together to calculate the comparisons shown in Figure S4.

Bone marrow derived macrophage (BMDM) cultures and ELISA.
CD45+ bone marrow cells were sorted by FACS (AriaI, BD Biosciences) from unlesioned isochronic-young, isochronic-old, or heterochronic parabiotic pairs (joined four weeks previously at 2 months or 24 months of age). Bone marrow cells were cultured at an initial density of $1x10^6$ cells/ml for 7 days, and differentiated in DMEM (high glucose) supplemented with 20% heat-inactivated FCS, 100u/ml pen-strep, 10mM sodium pyruvate (Gibco), 2mM GlutaMAX (invitrogen) and 50ng/ml M-CSF (R&D Systems).

Fresh media was added at days 3 and 5. To confirm the purity of macrophages in culture, the cells were double stained with fluorochrome–conjugated mAbs to the macrophage lineage markers F4/80 (BM8) and CD11b (Mac-1) (both from eBiosciences). Stained cells were analyzed using FACS (LSRII flow cytometer, BD Biosciences) and data were analyzed with FlowJo software (Tree Star). For LPS stimulation, cultured cells were harvested with 0.2% EDTA (Invitrogen) and plated at $4x10^5$ per ml in DMEM supplemented with 10% FCS. Macrophages were cultured for at least 12h after replating before stimulation with LPS (10ng/ml, from E.coli serotype 0111-B4, Sigma) for 6h. Cell-free supernatants were collected, snap frozen and stored at -80^{o}c until use. Growth factors, including IGF-1, PDGF-A (both from R&D) and FGF basic (Abcam), were measured by ELISA, following the manufacturer's instructions.

Statistical analysis. All statistical analysis was performed in GraphPad Prism (GraphPad Software, Inc.). For data derived from the quantification of immunohistochemical staining, comparisons between two groups were performed with an unpaired t-test assuming two-tailed distribution and equal variances. In cases where more than two groups were compared to each other, a one-way analysis of variance (ANOVA) was performed assuming equal variances, followed by an appropriate post-test to compare individual groups. For ranking analysis of remyelination, the non-parametric Mann-Whitney test was used to determine whether two groups differed in their extent of remyelination. A comparison of the extent of remyelination between three groups was performed using a Kruskal-Wallis test followed by Dunn's post test to compare individual groups. For the cytokine arrays, statistical analysis was performed using one-way ANOVA followed by Bonferroni's Multiple Comparison Test. Finally, comparison of growth factor production by BMDM was performed using Kruskal-Wallis followed by Dunn's post-test. For all statistical tests, differences were considered significant at $p<0.05$.

SUPPLEMENTAL REFERENCES

Arnett, H.A., Fancy, S.P.J., Alberta, J.A., Zhao, C., Plant, S.R., Raine, C.S., Rowitch, D.H., Franklin, R.J.M., and Stiles, C.D. (2004). The bHLH transcription factor Olig1 is required for repair of demyelinated lesions in the CNS. Science *306* 2111-2115.

Boring, L., Gosling, J., Chensue, S.W., Kunkel, S.L., Farese, R.V., Jr., Broxmeyer, H.E., and Charo, I.F. (1997). Impaired monocyte migration and reduced type 1 (Th1) cytokine responses in C-C chemokine receptor 2 knockout mice. J Clin Invest *100*, 2552-2561.

Wagers, A.J., Sherwood, R.I., Christensen, J.L., and Weissman, I.L. (2002). Little evidence for developmental plasticity of adult hematopoietic stem cells. Science *297*, 2256-2259.

Woodruff, R.H., Fruttiger, M., Richardson, W.D., and Franklin, R.J.M. (2004). Platelet-derived growth factor regulates oligodendrocyte progenitor numbers in adult CNS and their response following CNS demyelination. Molecular and Cellular Neuroscience *25*, 252-262.

Wright, D.E., Wagers, A.J., Gulati, A.P., Johnson, F.L., and Weissman, I.L. (2001). Physiological migration of hematopoietic stem and progenitor cells. Science *294*, 1933-1936.